AIP | Review of Scientific Instruments

Molecular beam apparatus with supersonic O2 beam (700–3000 m/sec) for reactive scattering experiments with metal atoms

C. B. Cosmovici, K. W. Michel, R. Dirscherl, and U. Stanggassinger

Citation: Review of Scientific Instruments **47**, 667 (1976); doi: 10.1063/1.1134719
View online: http://dx.doi.org/10.1063/1.1134719
View Table of Contents: http://scitation.aip.org/content/aip/journal/rsi/47/6?ver=pdfcov
Published by the AIP Publishing

Molecular beam apparatus with supersonic O_2 beam (700–3000 m/sec) for reactive scattering experiments with metal atoms

C. B. Cosmovici,* K. W. Michel, R. Dirscherl, and U. Stanggassinger

Max-Planck-Institut für Physik und Astrophysik, Institut für extraterrestrische Physik, 8046 Garching, West Germany

(Received 25 August 1975; in final form, 14 November 1975)

Design and performance of a heatable, easily alignable Pt-nozzle source (pinhole) are described, providing sufficient O_2 intensity in both pure gas and seeded beam operation for crossed beam experiments with metal atoms and mass spectrometric detection. At the chosen skimmer-nozzle distance, nozzle Knudsen numbers around $K_n \simeq 10^{-2}$ gave optimum velocity ratio and intensity for all gas mixtures at nozzle temperatures from 300 to 1300 K. The oven design is particularly suited for effusive metal beams at $T < 1200$ K.

I. INTRODUCTION

In the attempt to develop the molecular beam technique to its limits and to leave the so-called "alkali age," much effort has been devoted to the design and operational refinements of mass spectrometric detection systems.[1,2]

Generally, this involves carefully chosen noise suppression techniques and differentially pumped detector chambers, which involve complexity and stringent requirements of mechanical stability. Much valuable information can be derived, however, even with low-cost equipment if full use of modulated nozzle sources is made.

Nozzle beams provide the advantage of high flux density, narrow velocity distribution, and wide range of collisional energies which can be covered, thus meeting best the present demand for specified differential cross sections. The basic principles of nozzle expansions into a vacuum, i.e., nearly isentropic conversion of thermal into directed flow energy, have been known for a long time and even the efficiency of rudimentary nozzles has been documented as early as 1954.[3] It was, however, not before the mid 1960s that detailed investigations of the angular flow pattern[4] and of the actual velocity distribution[5] established confidence in the method. Still, overestimate of pumping capacity and of requirements as to nozzle shaping, in conjunction with difficulties in beam alignment, prevented a widespread use and full appraisal of the versatility of the technique, the potential of which is considerably enhanced when using seeded beams.[5] The application of nozzle jets as a cheap and reliable working tool resides on further work on optimum skimmer design,[6] on jet–skimmer interference,[7] on diffusive separation in a two-component jet,[8] and on a neat description of the velocity distributions.[9]

In the following we describe a simple and easily alignable nozzle source, withstanding corrosive O_2 and consisting of a pinhole in a heatable platinum tube, which in conjunction with a thermal oven beam allows continuous variation of collisional energies from 0.1 to 1 eV. This energy range is of particular interest in reaction kinetics, because it becomes comparable with typical energies of chemical bonding so that both bond dissociation energies can be determined[10] and the effect of energy on reaction dynamics can be studied.[11] At optimum performance, the intensity of the present beams was high enough to study chemical exchange reactions with cross sections down to 10^{-17} cm^2 even with a rotatable mass spectrometer detector of notoriously low efficiency.

One of the basic principles for the design of a molecular beam apparatus for achieving reactive high-energy collisions is that the light collision partner should be accelerated by entrainment in a largely abundant carrier gas in the nozzle expansion, whereas the heavy reactant may well be a thermal beam from an effusive oven source. This has occasionally been overlooked, because, seen in the laboratory frame of reference, the kinetic energy of the heavy solute molecule in the carrier gas certainly is nearly proportional to its molecular weight[5]; the relative collisional energy E, however, which is the quantity of interest, is practically only determined by the maximum gasdynamic velocity for steady expansion of the carrier gas into vacuum

$$v(O_2) \approx v_{\max}(He) = \left(\frac{2\gamma}{\gamma - 1} \frac{RT_N}{\langle m \rangle} \right)^{1/2}, \qquad (1)$$

since

$$E = \tfrac{1}{2}\mu[v^2(O_2) + v^2(M)], \qquad (2)$$

with the notation γ equal to the ratio of specific heats in the nozzle expansion, T_N the nozzle temperature, $\langle m \rangle$ the average molecular weight of the mixture, and μ the reduced mass of oxygen molecule and collision partner M. Furthermore, it is obvious from Eq. (2) that the width of the distribution of relative collisional energies is dominated by the spread in velocities of the nozzle jet if $v(O_2) \gg v(M)$, whereas the thermal spread in the oven beam scarcely affects the results. Hence, if possible heavy metal atoms should be chosen for the oven source.

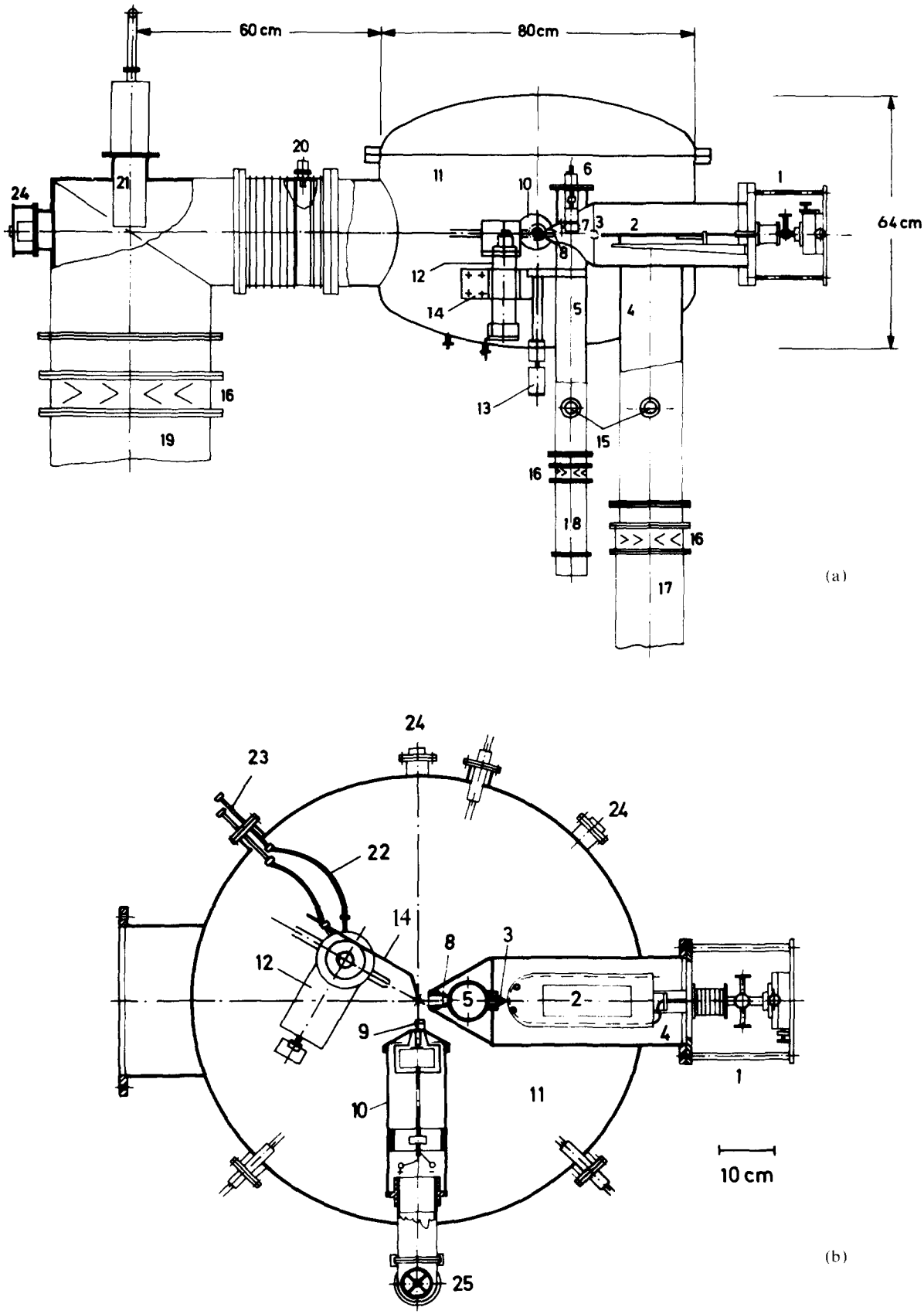

FIG. 1. Molecular beam apparatus (MSA). (a, b)—Side and top views: 1—Nozzle alignment; 2—platinum tube support; 3—skimmer; 4—nozzle chamber (10^{-2}–10^{-6} Torr); 5—collimation chamber (10^{-4}–10^{-6} Torr); 6—chopper alignment; 7—chopper with lamp and photocell; 8—collimator; 9—solenoid activated beamflag; 10—oven chamber (10^{-4}–10^{-6} Torr); 11—scattering chamber (10^{-6}–10^{-8} Torr); 12—quadrupole mass spectrometer (QUAD); 13—rotary feed through; 14—rotatable table for the QUAD; 15—Penning gauge; 16—cooled baffles; 17—oil diffusion pump (Leybodiff 1000/4); 18—oil diffusion pump (Leybojet 170 L); 19—oil diffusion pump (Leybold DI-3000); 20—ionization vacuum gauge (IM-VI-Leybold); 21—cryopump (Balzers 1000); 22—flexible bellows; 23—LN_2 feed through; 24—window; 25—oil diffusion pump (Leybodiff 170).

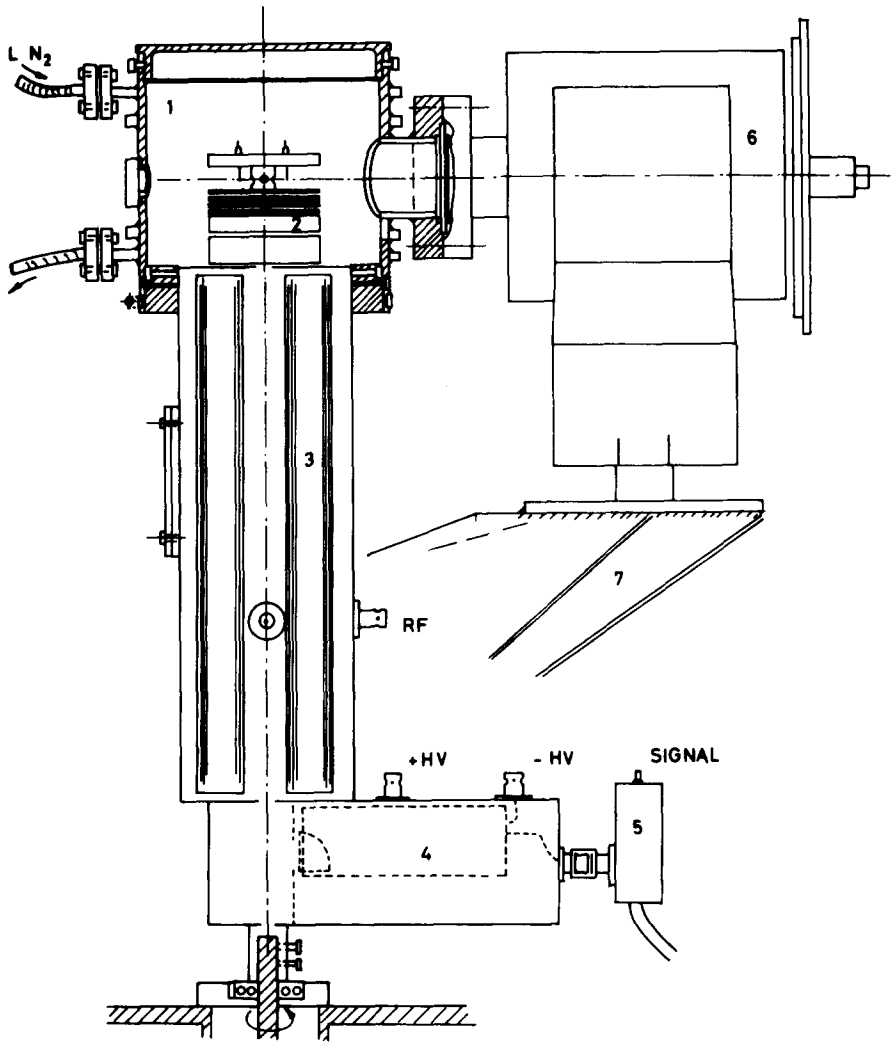

FIG. 2. Detection system: 1—Ionizer chamber (10^{-6}–10^{-9} Torr); 2—ionizer; 3—quadrupole; 4—electron multiplier; 5—preamplifier; 6—ion pump (15 liter/sec—Varian); 7—rotatable table.

Another reason for accelerating the light collision partner is the ensuing high accuracy in the velocity analysis of the reaction products. The product velocity in the center-of-mass system is the typical information derived from reactive molecular beam scattering. If, however, the heavy partner is accelerated, the center-of-mass vector points almost in the same direction as the fast reactant beam. Then, apart from poisoning effects on the detector, angular product distribution curves are extremely difficult, if not impossible, to interpret because of lack in angular resolution, as is immediately obvious from inspection of the corresponding kinematic diagrams.

The present arrangement was chosen so that the center-of-mass vectors were far from the reactant beams, which thus did not interfere with product distribution curves.

II. APPARATUS DESCRIPTION

Figures 1 and 2 show the apparatus (sectional view and top view) and the detector. The molecular beam system (here called MSA) consists of five stainless-steel vacuum chambers which are separately pumped: (a) the nozzle chamber, (b) the collimator chamber, (c) the oven chamber, (d) the ionizer chamber, and (e) the scattering chamber.

This configuration has been used to study reactive scattering between thermal metal atoms (Ba, Sr, and Eu) and supersonic O_2. For other studies, the thermal oven can be replaced by another nozzle system.

A. Vacuum system

A combination of two mechanical pumps (Ruvac ZO5 and D 25 Leybold) backs Leybold oil diffusion pumps supplied with LN_2 (78 K) and Freon-cooled baffles (−30°C). Table I shows the vacuum conditions in the four chambers. In the diffusion pumps pure hydrocarbon oil was used (Diffelen ultra Leybold; vapor pressure at 20 °C, 5×10^{-8} Torr; SiO_2 deposits from silicon oil would have poisoned the dynodes of the open electron multiplier). A cryopump (Fig. 1, 21) (Balzers 1000 liters/sec), installed in the scattering chamber on the axis of the nozzle beam, was used only for very sensitive measurements in the 10^{-8} Torr range. The lid of the scattering chamber (diameter–80 cm; heatable to 150 °C) could be removed easily by a gallows

TABLE I. Vacuum conditions.

Chamber	Gas load (liter/sec)	Pumping[a] velocity (liter/sec)	Measured pressure (15 and 20 of Fig. 1) (Torr)
Nozzle	300	400	10^{-3}–10^{-4}
Collimator	100	118	10^{-5}
Oven	70	118	10^{-5} (with metal evaporation)
Scattering	1000	1870	3×10^{-7} (8×10^{-7} with metal evaporation)
Ionizer		15	$<10^{-8}$

[a] At $P < 6 \times 10^{-4}$ Torr.

for operations inside the chamber, and was sealed by means of a Viton O-ring. Before opening, all chambers were flooded with Ar in order to avoid deposits of H_2O and oxidation of both the Cu–Be dynodes of the electron multiplier and the metal to be evaporated in the oven. An automatic control system puts the diffusion pumps into operation only at vacua better than 5×10^{-2} Torr and at sufficient supply of cooling water. In the case of a current failure the UHV system is protected by an electropneumatic valve. Finally, the control system does not permit the quadrupole mass spectrometer to be turned on before a high vacuum is reached in the scattering chamber thus preventing arc discharges at the high frequency (1.2 MHz) and the high-voltage (7000 V) cables and to avoid burning out the ionizer filament.

The pressure in the vacuum system is measured by Thermotrongauges (Leybold) in the range 10^{2}–10^{-2} Torr, by Penning gauges (Leybold) in the range 10^{-2}–10^{-6} Torr, and by ionization gauges (IM-VI-Leybold) in the range 10^{-4}–10^{-8} Torr.

B. Nozzle system

The most important part of the molecular beam apparatus is the nozzle system. Figure 3 shows the schematic side view. The nozzle is only a pinhole of about 100 μ diameter (micrograph in Fig. 4) bored by means of a ruby laser (Siemens) in the wall of a thin platinum tube (thickness 0.25 mm). This U-shaped tube (1.5 mm o.d., 1.0 mm i.d., length 50 cm) is closed on one end (Fig. 4); the open end is connected with the gas inlet. For support, the platinum tube lies between two stainless steel plates (Fig. 4, 3) and is insulated by means of ceramic beads.

The nozzle can be heated directly. The terminals for up to 30 A ac heating current, resulting in temperatures up to 1500 K, are situated 1 cm from the nozzle thus minimizing the surface to be heated. Platinum was chosen for four reasons: (1) high melting point (1774°C); (2) inertness to corrosive gases; (3) easy to work on; (4) fair resistivity. The temperature can be measured with a thermocouple which is situated 2 mm from the nozzle or optically by means of a pyrometer (Pyrowerk $\lambda = 6560$ Å). Two micrometer screws on the outside (see 8, Fig. 3) allow a perfect alignment of the nozzle beam with the skimmer and the collimator (see below).

Gas inlet (Fig. 3, 6) and heating (Fig. 4, 10) take place through the same copper tube soldered to the platinum tube. A stainless steel bellows serves as a flexible seal (Fig. 3, 5). In order to exchange

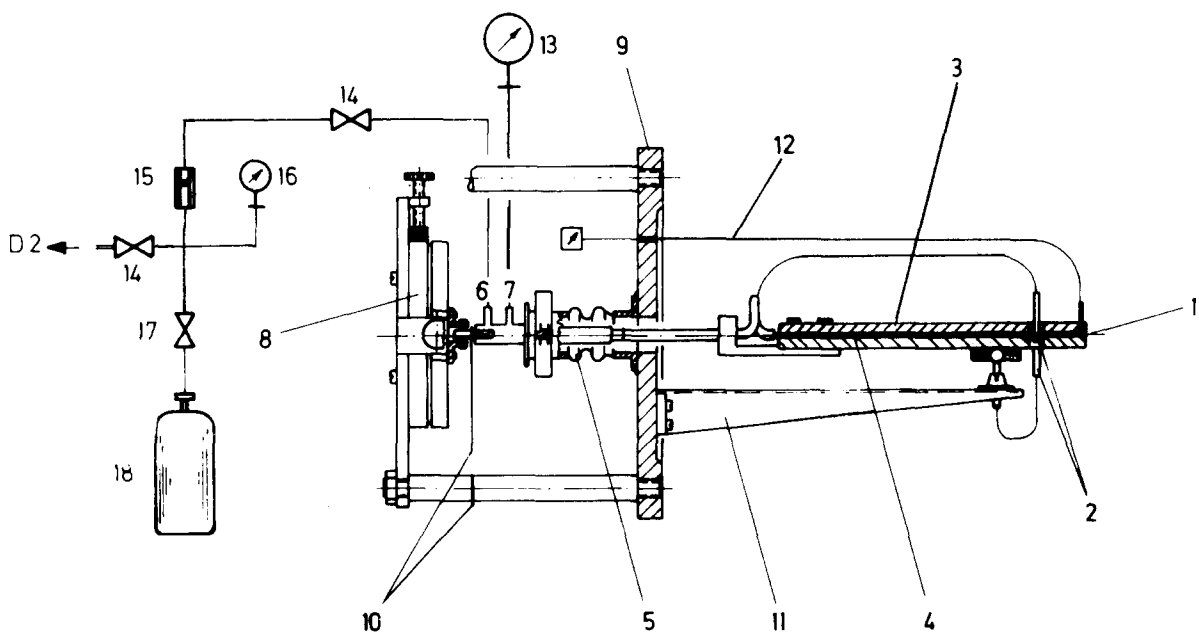

FIG. 3. Nozzle alignment: 1—Nozzle; 2—electrical clamps; 3—stainless steel plates; 4—platinum tube; 5—stainless steel bellows; 6—gas inlet; 7—connection for pressure gauge; 8—alignment device; 9—flange; 10—electrical clamps; 11—support; 12—thermocouple; 13—pressure gauge; 14—valve; 15—flowmeter; 16—pressure gauge; 17—valve; 18—gas bottle.

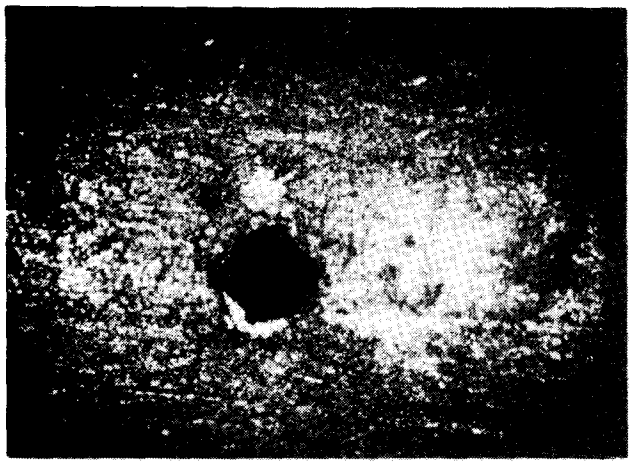

FIG. 4. Platinum tube with nozzle.

the gas in the entire nozzle system quickly, this can be evacuated separately with a small mechanical pump (D2—Leybold) (Fig. 3, 14).

C. Collimator chamber

The nozzle chamber is separated from the collimator chamber by a skimmer (Fig. 5, 7), the geometric details being specified in Table II. A screw thread allows variation of the distance between skimmer tip and nozzle from 0 to 20 mm.

The skimmed nozzle beam is then chopped by a rotating disk at a frequency between 10 and 1000 cycles/sec (vacuum motor of type Escap 26, continuously variable rpm up to 4300). The modulation frequency can be increased by increasing the number of slots in the exchangeable rotating disk. The chopper system can be moved up and down for good alignment with the beam (Fig. 6, 4). A phototransistor (BPX 25 Valvo) and a straight-filament lamp (Fig. 6, 6) supply the reference signal for the phase-sensitive measurements. The exact phase angle between beam (detector signal) and the reference signal had to be obtained on the basis of time-of-flight measurements (see below). Generally, the alignment of the chopper was made with a He–Ne laser beam instead of the nozzle beam.

In this way an almost monoenergetic and modulated nozzle beam of known shape and flux density reaches the scattering chamber through a collimator, which is also movable on the beam axis, and whose geometry is given in Table II. The divergence of the beam does not exceed 2° (FWHM).

Unlike the skimmer, the collimator has rectangular slit of 1 × 6 mm which is not, as usual, cut in a flat, but rather in a bow-shaped surface in order to avoid a gas cushion between chopper and collimator (see Fig. 5).

D. Oven chamber

Vaporization occurs at temperatures up to 1200 K in a stainless steel oven shown in Fig. 6. Table III shows metals which develop in this oven a vapor pressure of at least 10^{-1} Torr, thus yielding sufficiently intense vapor jets for scattering experiments. The cylindrical oven has double walls which leave sufficient space between them (Fig. 6, 1) for a coaxial bifilar wire (Philips Typ ZE), closely wound in milled-in grooves (Fig. 6, 9). The space between the walls is hermetically sealed by welding seams. A feed-through insulator, separated from the oven by a long shell (Fig. 6, 3) for thermal protection, ($T \approx 100$°C) provides the one electric terminal, the other one being grounded. To obtain a temperature gradient, heating wire and lead-in wire should have a resistance ratio of 20:1, thus making the usual provisions for cooling unnecessary. By means of a dc heating current of 1.7 A at 120 V

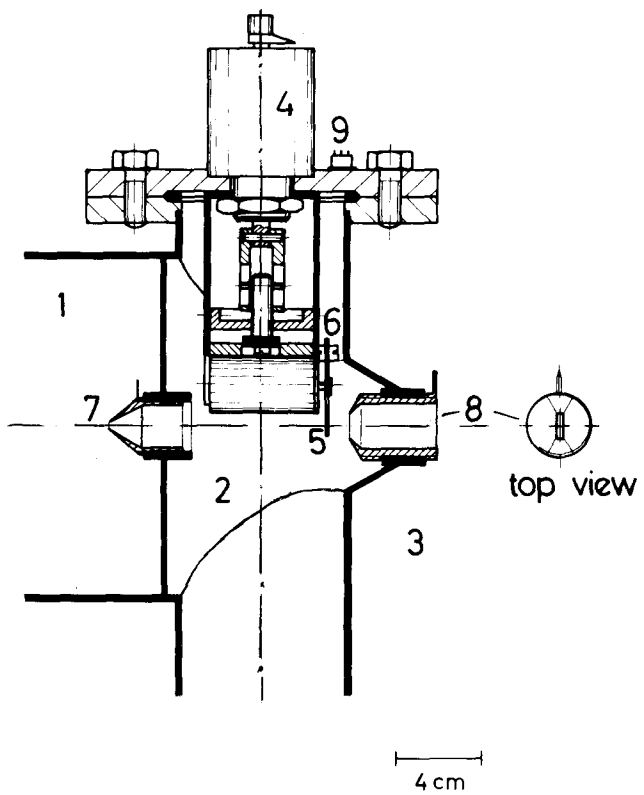

FIG. 5. Collimator chamber: 1—Nozzle chamber; 2—collimator chamber; 3—scattering chamber; 4—alignment device; 5—chopper; 6—lamp and phototransistor; 7—skimmer; 8—collimator; 9—electrical clamps.

TABLE II. Geometrical parameters in the nozzle beam system.

Nozzle diameter	0.1 mm	
Skimmer diameter	1.0 mm	
Skimmer geometry	40°	half-angle (inside)
	45°	half-angle (outside)
Collimator geometry	1 × 6 mm	
	60°	half-angle (inside)
	30°	half-angle (outside)

Distances	
Nozzle–skimmer	3 mm
Skimmer–chopper	110 mm
Chopper–collimator	10 mm
Collimator–scattering center	50 mm
Nozzle–scattering	183 mm
Scattering center–ionizer	258 mm
Chopper–ionizer	318 mm

one reaches an oven temperature of 1000 K (dc power supply, Harrison 6443 B, HP).

In order to minimize the heat losses by conduction, the oven is supported only by four ceramic pedestals (Fig. 6, 2), the alignment being secured by a ceramic clamp at the shell (Fig. 6, 8).

The oven aperture is circular with a diameter of 8 mm; this value was chosen to facilitate feeding of the oven with larger bars of the metal to be evaporated. On the other hand, it sets an upper limit to the vapor pressure of 10^{-1} Torr, because the original Maxwellian velocity distribution, assumed to hold in the reduction of scattering data, would be falsified if the orifice diameter exceeds the mean free path appreciably (nozzle effect).

An interchangeable slit (5 × 8 or 3 × 8 mm) (Fig. 6, 5,6) was cut into the front cover of the oven chamber and serves to define the atomic beam and hence the dimensions of the scattering volume. The atomic beam can be interrupted by a solenoid-activated beam flag (Fig. 6, 12).

The oven temperature is determined by optical pyrometry, and mass-loss rates, obtained by weighing before and after a series of runs, are in agreement with the vapor pressure corresponding to this temperature. Thus, the properties of the vapor beam seem to be described adequately by the expressions of kinetic theory of gases for an ideal orifice (see Ref. 12 for latest discussion of deviations and further references). By moving the entire oven chamber, the distance between orifice and the nozzle beam can be varied from 10 to 4 cm.

E. Detection system

A quadrupole mass spectrometer (Extranuclear Lab. Inc.) with cross-beam ionizer and 14-dynode Cu–Be electron multiplier (off-axis, perpendicular mounting) is used as universal detector for all atomic and molecular species in the mass range 1–350 amu (electron energy, 1–100 eV; emission current, up to 50 mA; ionization probability, $\simeq 10^{-3}$; EM typical gain $\simeq 10^5$ at 3 kV).

The new and satisfactory application of this widely used detection system consists in mounting it on a rotatable table (see Fig. 1, 26) in the scattering chamber with differentially pumped ionizer. The quadrupole detector can be rotated in the plane of the beams, covering a range of scattering angles of about 130° with an accuracy of ±0.5°.

It is mounted perpendicular to the beams (cross-beam operation), so that the nonionized particles can pass through the ionizer without contaminating the quadrupole rods and the electron multiplier. The distance between detector and scattering center can be varied from 8 to 28.5 cm; this is of great advantage for time-of-flight measurements on fast seeded beams.

Thus, with the same apparatus, both velocity distributions in dense primary beams and angular distributions of scarce product molecules can be measured.

In order to minimize poisoning effects caused by the metallic atom beam and to increase the S/N ratio, a differentially pumped chamber was constructed around the ionizer. It consists of a circular stainless steel cylinder surrounding the ionizer, with removable top, pumped by a 15-liter/sec ion pump (Varian) (see Fig. 2). The chamber can be cooled to LN_2 temperature, thus acting as a cold trap for condensibles.

Collimating apertures for variable length and diameter for the incoming as well as for the outgoing beam are provided. The ionizer chamber thus permits a vacuum improvement around the ionizer by one order of magnitude with respect to the scattering chamber.

The advantages achieved hereby are

(1) negligible fluctuations of the signal due to variations in background pressure;

(2) negligible poisoning of the ionizer;

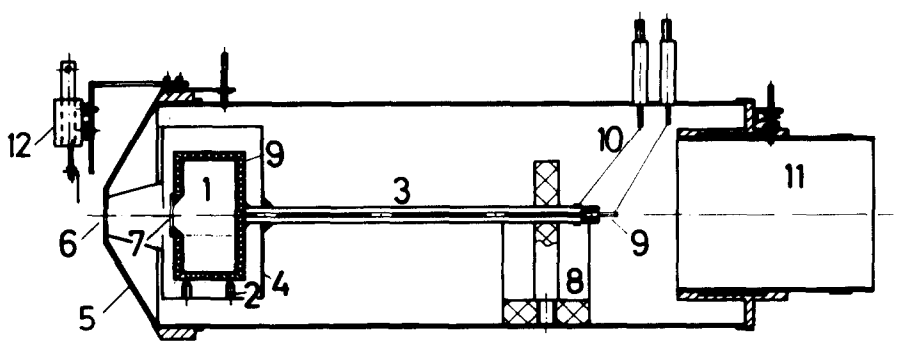

FIG. 6. Oven chamber: 1—Oven; 2—ceramic insulators; 3—support for the bifilar heating wire; 4—heat shield; 5—lid; 6—slit (5 × 8 mm); 7—oven orifice (diam, 8 mm); 9—bifilar heating wire; 10—electrical clamps; 11—support for the oven chamber; 12—solenoid-activated beam flag.

TABLE III. Reactions of metals with O_2 which can be studied with the present experimental setup.

Oxide (MO)	Reaction	Do (eV)	Ref.	T (K) at $Pv = 10^{-1}$ Torr	
BaO	Exo	5.75 ± 0.15	20	984	*
EuO	Endo	5.00 ± 0.02	19	981	
YbO	?	5.3 ± 1.5	20	920	
CaO	Endo	4.78 ± 0.87	18	962	*
SrO	Endo	$4.88^{+0.15}_{-0.03}$	10	850	*(?)

Do: dissociation energy from vibrational ground state.
Exo: exothermic; Endo: endothermic.
Pv: vapor pressure of metal.
* : Observed in Sun or stellar photospheres.

(3) a large increase of the measurable scattering angle (-10, $+120°$, $0°$ being the primary beam position);
(4) an increase of the S/N ratio by a factor of 20.

For measurements of the velocity distribution of the nozzle beam (Fig. 7), an emitter follower of time constant 10 μsec was attached directly to the electron multiplier. The output signal was recorded either on an oscilloscope or by means of a lock-in amplifier (PAR 124).

III. PERFORMANCE

Since the main purpose of this construction was to achieve a wide range of velocities, a high intensity and a narrow velocity distribution of the nozzle beam, the vacuum conditions (Table I), the geometry of the nozzle system (Table II), and the nozzle beam characteristics (Table III) have been accurately studied in order to obtain a beam whose properties were very close to those predicted by the theory.

Density, mass flow, flux, flux density, Knudsen number, and L number were calculated on the basis of the following equations:

(1) Density ρ_0 on the axis[4]:

$$\frac{\rho(R,\vartheta)}{\rho_0(R,0)} = \cos^2\left(\frac{\pi}{2}\frac{\vartheta}{\phi}\right), \tag{3}$$

with the maximum flow angle of the Prandtl–Mayer expansion

$$\phi = \frac{\pi}{2}\left[\left(\frac{\gamma+1}{\gamma-1}\right)^{1/2} - 1\right]. \tag{4}$$

The ratio of specific heats, γ, is determined by assuming additivity of the specific heats, weighted by their mole fractions. For O_2 we recognize that the vibrations will not relax during the expansion ($\gamma_{O_2} = 1.4$).

(2) Mass flow $\dot{m}$ and flux $\dot{n}$ ($= \dot{m}A/M$, with A the Avogadro number and M the mass number)[13]:

$$\dot{m} = P_N D\Gamma/(RT_N)^{1/2}, \tag{5}$$

where P_N and T_N are the pressure and temperature in the nozzle, and D is the surface of the nozzle.

$$\Gamma = (\gamma)^{1/2}\left(\frac{2}{\gamma+1}\right)^{(\gamma+1)/2(\gamma-1)}. \tag{6}$$

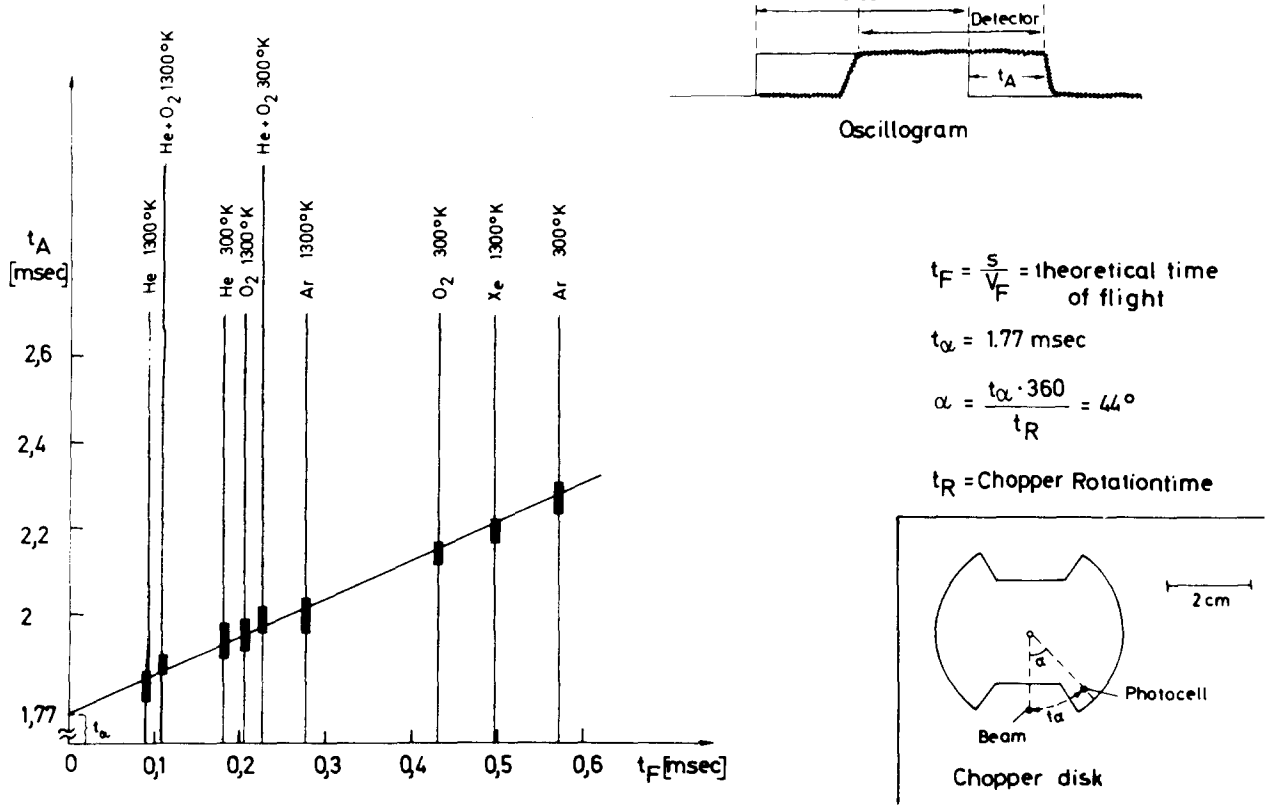

FIG. 7. Determination of t_α and chopper-disk geometry.

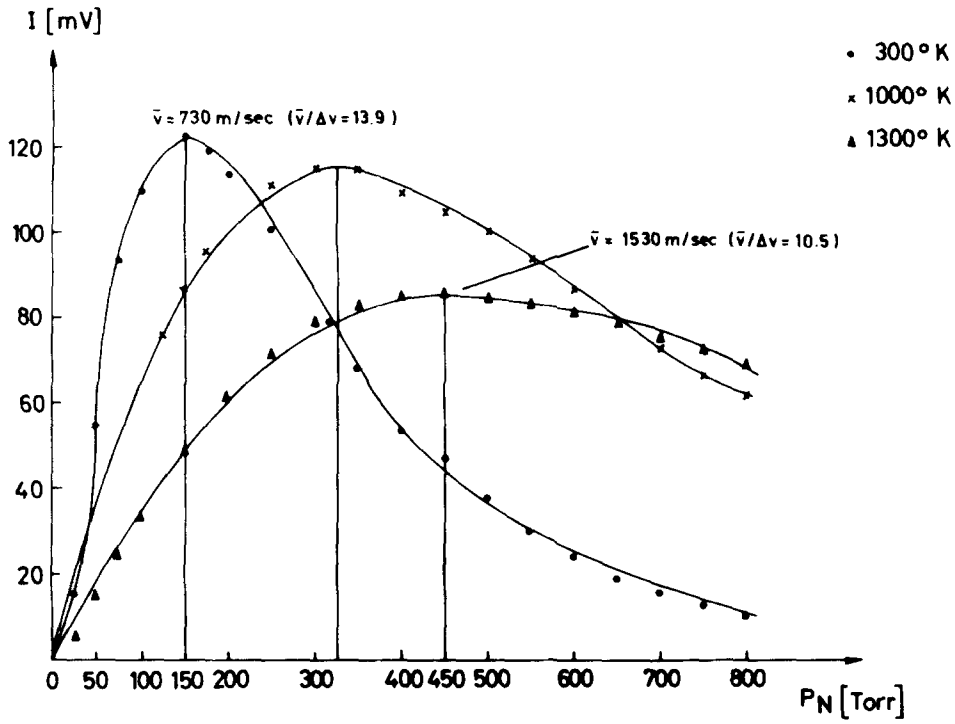

FIG. 8. Modulated O_2 nozzle beam. On the abscissa the nozzle pressure is plotted and on the ordinate the beam intensity measured with lock-in amplifier (R = 1 MΩ).

(3) The flux density I can be calculated from Eq. (3) by integration from O to ϕ[13]:

$$I = \rho_0 v = \dot{n}/(x^2 \cdot 4.89) \quad \text{for the } O_2 \text{ beam,}$$
$$= \dot{n}/(x^2 \cdot 3.6) \quad \text{for the seeded beam,} \tag{7}$$

with x equal to the distance from the nozzle (see Table II).

(4) Knudsen number: For an adiabatic flow K_n is given by[13]

$$K_n = \frac{\lambda^*}{d} = \frac{kT_N}{\sqrt{2}\pi d_G^2 d P_N [2/(\gamma+1)]^{1/\gamma-1}}, \tag{8}$$

where λ^* is the mean free path in the nozzle, d is the nozzle diameter equal to 100 μ, d_G = 3.35 Å is the gas kinetic diameter of the molecules, which has been taken uniformly even though this value depends on the gas mixture and on the effective temperature.

(5) L number, i.e., the axial nozzle distance below which a continuum flow can be assumed[14]:

$$L = d \cdot 0.238 K_n^{-0.6}. \tag{9}$$

IV. NOZZLE BEAM MEASUREMENTS

The seeded beam technique, which consists of accelerating heavier atoms or molecules by lighter atoms was applied successfully to a mixture of O_2 (9%) and He (91%). The beam density in dependence of pressure (P_N) and temperature (T_N) in the nozzle was determined for the gases O_2, Ar, He, Xe, Ne, and He + O_2.

In Figs. 8 and 9 the measured beam density for O_2 and He + O_2 at various temperatures is plotted as a function of stagnation pressure. The rise of the curves at increasing pressures P_D is caused by the decrease of the Knudsen numbers which are inversely proportional to P_D [see Eq. (8) and Table IV]. The intensity decrease after reaching a maximum is caused by the skimmer interference.[15] This effect appears when the gas mole-

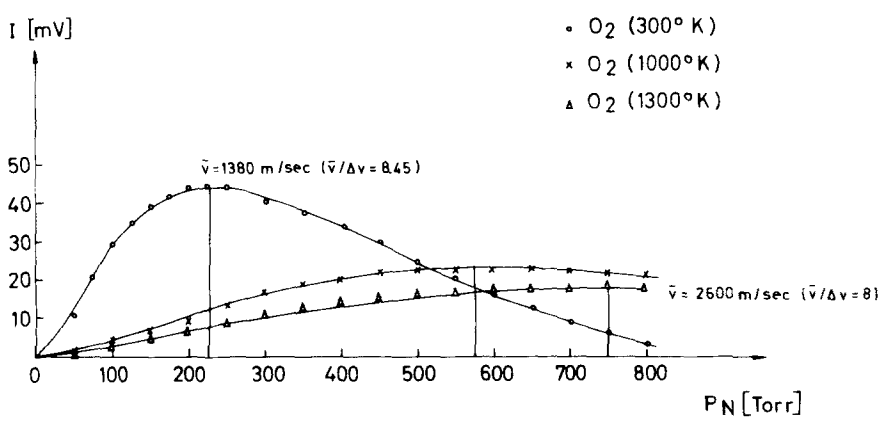

FIG. 9. Modulated O_2 nozzle beam (seeded). He + O_2 (91% + 9%).

TABLE IV. Nozzle beam characterization.

	γ	Γ	P_N	v_{eq}	K_n	$\dot{m}$	$\dot{n}$	I (S)	I (I)	ρ (S)	ρ (I)	I (mV)	L
A	1.4	0.685	150	738	6.5×10^{-3}	3.9×10^{-4}	0.74×10^{19}	4.5×10^{15}	2.28×10^{15}	6.1×10^{10}	3.1×10^{10}	120	0.134
B	1.4	0.685	450	1537	9.4×10^{-3}	5.2×10^{-4}	0.98×10^{19}	6.0×10^{15}	3.03×10^{15}	3.9×10^{10}	2.0×10^{10}	80	0.131
C	1.63	0.720	750	2930	17.2×10^{-3}	9.3×10^{-4}	1.79×10^{19}	1.45×10^{16}	7.3×10^{15}	4.9×10^{10}	2.5×10^{10}	20	0.126

A: O_2 beam at 300 K; B: O_2 beam at 1300 K; C: O_2-seeded beam at 1300 K.
Γ from Eq. (6); v_{eq}(m/sec) from Eq. (1); K_n from Eq. (8); $\dot{m}$ (g/sec) from Eq. (5); $\dot{n}$ (molecules/sec) from Eq. (5); I(molecules/cm² sec) from Eq. (7); ρ (molecules/cm³) from Eq. (7); L(cm) from Eq. (9).
(S): in the scattering center; (I): at the ionizer.
P_N: optimum nozzle pressure from Figs. 8 and 9.
I (mV): measured signal intensity from Figs. 8 and 9.

cules, which are reflected from the skimmer surface, are not pumped off quickly enough, and interfere with the nozzle beam, destroying its original shape. The mean velocity $\bar{v}$ and the velocity spread Δv of the nozzle beam were measured with the following procedure.

V. DETERMINATION OF MEAN VELOCITY $\bar{v}$ AND OF VELOCITY SPREAD Δv

The chopper reference signal and the emitter follower signal (connected with the QUAD electron multiplier) were simultaneously registered from a two-channel oscilloscope by means of a polaroid camera.

The noise of the detector signal could be averaged out by long integration time (exposure time, 10 sec), i.e., the beam crossed the screen 2000 times for one picture at the same trigger position.[11,13] Those registrations were repeated several times for each point of the intensity curves of the various gases in order to control the experimental error. The mean velocity is given by $\bar{v} = s/t_M$, with s (=31.8 cm) the distance between chopper and detector and $t_M = t_A - t_\alpha$; t_A is the time difference between detector and reference signal, and t_α is the time that a given point of the chopper disk needs to cover the distance between phototransistor and nozzle beam (see Fig. 7).

In order to determine t_α to an accuracy of ± 10 μsec it was necessary to evaluate the angle α up to an accuracy of 0.05° which cannot be attained by a direct mechanical measurement. Therefore, t_α was determined experimentally as follows: In a diagram (Fig. 7) the measured values of t_A for slower and quicker gases at 300 and 1300 K) were plotted against the corresponding times of flight $t_F = S/v_F$. It has been assumed here that v_F corresponds to the theoretical equilibrium velocity v_{eq} [Eq. (1)]. The point where the straight line cuts the t_A axis ($t_F = 0$), i.e., the gradient of this straight line gives with a good accuracy the t_α value.

The maximum values of $\bar{v}$ thus obtained agree very well with the theoretical v_{eq}, as Table V shows.

The deviation between $\bar{v}$ and v_{eq} amounts to about 1%–2% for O_2 (300 K, 1300 K) and He + O_2 (300 K), whereas for He + O_2 (1300 K) the difference amounts to 11%. This confirms that for calculating the Knudsen numbers one should take different cross sections for He/O_2 and for pure O_2.[16]

Let us assume a symmetrical triangular distribution of the nozzle beam which corresponds quite well to a usually observed Gaussian distribution.[14]

The ratio $\bar{v}/\Delta v$ is given by[13]

$$\bar{v}/\Delta v \simeq 2s/\bar{v}\tau_F, \tag{10}$$

with

$$\tau_F \simeq \tau - \tau_s \cdot t_Q/t_s.$$

τ is the rise time of the detector signal measured at the quickest rotation time (t_Q = 14.55 msec), τ_s is the rise time of the quickest beam signal (He at 1300 K) at the slowest rotation time (t_s = 71 msec).

Equation (10) allows the determination of Δv since $\bar{v}$, τ, and τ_s can be measured directly from the analysis of the oscillograms. The maxima for the values $\bar{v}/\Delta v$ are given in Table V and plotted in Figs. 8 and 9. The error for $\bar{v}/\Delta v$ is given mostly by the error in the determination of τ and τ_s.

Much more noise, caused by the lower intensity (see Fig. 9), was registered on the oscillograms of the He + O_2 beams and the error is thus about 10% higher.

Nevertheless, it can be seen that the concept of the nozzle construction has been successful, since the largest amount of the thermal initial energy is transformed into directed flow energy. In addition, the residual temperature T_R of the gas in the jet can be nominally determined from the conservation of energy law,

$$H_0 = [\gamma/(\gamma - 1)]RT_0 = \tfrac{1}{2}M\bar{v}^2 + [\gamma/(\gamma - 1)]RT_R, \tag{11}$$

TABLE V. Measured mean velocity $\bar{v}$ and maximum velocity spread $\bar{v}/\Delta v$.

T (K)	Gas	P_N (Torr)	$K_n \times 10^{-3}$	v_{eq} (m/sec)	$\bar{v}$ (m/sec)	$(v/\Delta v)_{max}$	$v/\Delta v$ from Eq. (13)
300	O_2	150	6.56	738	730	13.9 ± 20%	44.7
1300	O_2	450	9.45	1537	1530	10.5 ± 20%	69.2
300	He + O_2	220	10.8	1410	1380	8.4 ± 30%	27.2
1300	He + O_2	750	17.2	2930	2600	8.0 ± 30%	11.0

with

$$[\gamma/(\gamma - 1)]RT_0 = \tfrac{1}{2}Mv_{eq}^2,$$

and H_0 the enthalpy; it follows that

$$T_R = \frac{1}{2}\frac{\gamma - 1}{\gamma}\frac{M}{R}v_{eq}^2\left(1 - \frac{\bar{v}^2}{v_{eq}^2}\right). \quad (12)$$

The measured Δv corresponds in effect to the mean thermal velocity in one direction (in relation to the center-of-mass velocity $\bar{v}$). According to Moelwyn-Hughes[17]

$$\Delta v = \left(\frac{1}{2\pi}\frac{RT_R}{M}\right)^{1/2}$$

$$\Rightarrow \frac{\Delta v}{\bar{v}} = \left[\frac{1}{2\pi}\frac{\gamma - 1}{2\gamma}\left(\frac{v_{eq}^2}{\bar{v}^2} - 1\right)\right]^{1/2}. \quad (13)$$

Inserting in Eqs. (12) and (13) the γ values (Table III) and the v values (Table V), we can calculate the residual temperature T_R and the $\Delta v/v$ ratios (last column, Table V). For O_2 at 300 K we obtain

$$T_R = 3 \text{ K} \quad \text{and} \quad \Delta v/\bar{v} = 44.7.$$

VI. DISCUSSION

The fact that the observed Δv differs from the calculated Δv from Eq. (13) is a further indication that the temperature (resp. thermal velocity distribution) is not isotropic at the freezing boundary in the transition flow region. This effect has been observed also by Torello.[9] Therefore, the definition of a Mach number in a nozzle beam, as previously often postulated,[5] is not suitable, and we prefer the expression $v/\Delta v$.

The fact that the He + O_2 values deviate from the ideal case, especially at high temperatures, can be understood on the basis of the high Knudsen numbers.

For comparison we can also express our $v/\Delta v$ values in terms of terminal parallel Mach numbers, which have been related to Knudsen numbers in the form (Anderson, 1974[5])

$$M_T = k' \cdot K_n^{-0.4}, \quad (14)$$

where k' is a constant incorporating the collision effectiveness: $k' = 1.17$ for argon[14]; $k' = 0.85$ for helium.[16] We obtain $k' = 1.74$ for O_2 and $k' = 1.47$ for He + O_2.

The ratio of calculated O_2 densities (Table III) for cases A and B (column 11) corresponds to the measured ratio (column 12), thus confirming again the applicability of Eq. (7) and the fact that vibrations of O_2 do not relax even at 1300 K. No agreement with predicted O_2 densities in the ionizer region and measured intensities (case C, column 11 and 12) is found for seeded beams. The measured values are lower by a factor of 5. This is probably due to enhanced skimmer interference with the heavy gas load in seeded beams, for which the pumping efficiency in the nozzle chamber is not enough. The perturbation of the seeded beam is also documented by the larger discrepancy between measured and equilibrium mean velocities ($\bar{v}$ and v_{eq}) and by the lower values of $v/\Delta v$ (Table V).

Whereas the maximum values of the beam intensities for O_2 at all temperatures (Fig. 8) correspond fairly well to the ideal unperturbed expansion, this seems not to be the case for the seeded beams (Fig. 9). Before the ideal values are reached, skimmer interference sets in. However, the $v/\Delta v$ values for the seeded beams show, that even with small (i.e., inexpensive) pumps useful high-velocity jets of O_2 can be obtained, which can be considered as sufficiently monoenergetic for most reaction kinetic studies.

* Present address: Laboratorio di Fisica Cosmica, Istituto di Fisica, Università di Lecce, 73100 Lecce, Italy.

[1] Y. T. Lee, J. D. McDonald, P. R. Le Breton, and D. R. Herschbach, Rev. Sci. Instrum. **40,** 1402 (1969).
[2] R. W. Bickes and R. B. Bernstein, Rev. Sci. Instrum. **41,** 759 (1970).
[3] E. W. Becker and K. Bier, Z. Naturforsch. **92,** 975 (1954).
[4] H. Ashkenas and F. S. Sherman, in *Rarefied Gas Dynamics*, 4th Symp., edited by J. M. de Leeuw (Academic, New York, 1966).
[5] J. B. Anderson, R. P. Andres, and J. B. Fenn, in *Advances in Chemical Physics* (Wiley-Interscience, New York, 1966), Vol. X; J. B. Anderson, in *Molecular Beams and Low Density Gas Dynamics*, edited by P. P. Wegener (Dekker, New York, 1974), pp. 1–91.
[6] V. Bossel, F. C. Hurlbut, and F. S. Sherman, in *Rarefied Gas Dynamics*, 6th Symp., edited by L. Trilling and H. Y. Wachman (Academic, New York, 1969).
[7] K. Bier and O. F. Hagena, in *Rarefied Gas Dynamics*, 4th Symp., edited by J. M. de Leeuw (Academic, New York, 1969).
[8] V. Aurich and K. Schügerl, Ber. Bunsen-Ges. **73,** 993 (1969); and Naturwiss. **59,** 120 (1972). M. Witthaus and K. Schürgerl, Ber. Bunsen-Ges. **73,** 383 (1969).
[9] G. Scoles and F. Torello, Meccanica **3,** 20 (1968); F. Torello, AIAA J. **9,** 1843 (1971).
[10] C. B. Cosmovici and K. W. Michel, Chem. Phys. Lett. **16,** 77 (1972).
[11] C. B. Cosmovici and K. W. Michel, Chem. Phys. Lett. **11,** 245 (1971); M. E. Gersh and R. B. Bernstein, J. Chem. Phys. **56,** 6131 (1972).
[12] R. T. Grimely, D. W. Muenow, and J. L. La Rue, J. Chem. Phys. **56,** 490 (1972).
[13] C. B. Cosmovici, MPI/PAE-Extraterr. 62 (1972), Munich.
[14] J. B. Anderson and J. B. Fenn, Phys. Fluids **8,** 780 (1965).
[15] R. L. Le Roy and T. R. Govers, Can. J. Chem. **48,** 927; **48,** 1743 (1970).
[16] U. Buck, M. Düker, H. Pauly, and D. Pust, in *Proceedings of the 4th International Symposium on Molecular Beams*, Cannes, 1973.
[17] E. A. Moelwyn-Hughes, in *Physical Chemistry* (Pergamon, Oxford, 1961), p. 40.
[18] B. de B. Darwent, "Bond Dissociation Energies in Simple Molecules," NSRDS-NBS 31 (Jan. 1970).
[19] R. Dirscherl, Ph.D. thesis, Technische Universität, München, 1975 (unpublished).
[20] A. G. Gaydon, in *Dissociation Energies* (Chapman and Hall, London, 1968), 3rd ed.